Publ. Astron. Soc. Japan (2014) 00(0), 1–10
doi: 10.1093/pasj/xxx000

arXiv:1611.01588v1 [astro-ph.HE] 5 Nov 2016

J-GEM Follow-Up Observations of The Gravitational Wave Source GW151226[1]

Michitoshi YOSHIDA[2], Yousuke UTSUMI,[2], Nozomu TOMINAGA[3,4], Tomoki MOROKUMA[5,4], Masaomi TANAKA[6,4], Yuichiro ASAKURA[7], Kazuya MATSUBAYASHI[8], Kouji OHTA[8], Fumio ABE[7], Sho CHIMASU[9], Hisanori FURUSAWA[6], Ryosuke ITOH[10,11], Yoichi ITOH[12], Yuka KANDA[10], Koji S. KAWABATA[2], Miho KAWABATA[10], Shintaro KOSHIDA[13], Naoki KOSHIMOTO[14], Daisuke KURODA[15], Yuki MORITANI[4], Kentaro MOTOHARA[5], Katsuhiro L. MURATA[16], Takahiro NAGAYAMA[17], Tatsuya NAKAOKA[10], Fumiaki NAKATA[13], Tsubasa NISHIOKA[18], Yoshihiko SAITO[11], Tsuyoshi TERAI[13], Paul J. TRISTRAM[19], Kenshi YANAGISAWA[15], Naoki YASUDA[4], Mamoru DOI[5,20], Kenta FUJISAWA[21], Akiko KAWACHI[9], Nobuyuki KAWAI[11], Yoichi TAMURA[5], Makoto UEMURA[2] and Yoichi YATSU[11]

[1]Based on data collected at the Subaru Telescope, which is operated by the National Astronomical Observatory of Japan.
[2]Hiroshima Astrophysical Science Center, Hiroshima University, Hiroshima 739-8526, Japan
[3]Department of Physics, Faculty of Science and Engineering, Konan University, Kobe, Hygo 658-8501, Japan
[4]Kavli Institute for the Physics and Mathematics of the Universe (WPI), The University of Tokyo, Kashiwa, Chiba 277-8583, Japan
[5]Institute of Astronomy, Graduate School of Science, The University of Tokyo, Mitaka, Tokyo 181-0015, Japan
[6]National Astronomical Observatory of Japan, Mitaka, Tokyo 181-8588, Japan
[7]Institute for Space-Earth Environmantal Research, Nagoya University, Chikusa-ku, Nagoya 464-8601, Japan
[8]Department of Astronomy, Kyoto University, Kitashirakawa-Oiwake Kyoto 606-8502, Japan
[9]Department of Physics, School of Science, Tokai University, Hiratsuka, Kanagawa 259-1292, Japan
[10]Department of Physical Science, Hiroshima University, Hiroshima 739-8526, Japan
[11]Department of Physics, Tokyo Institute of Technology, Meguro-ku, Tokyo 152-8551, Japan
[12]Nishi-Harima Astronomical Observatory, University of Hyogo, Hyogo 679-5313, Japan
[13]Subaru Telescope, National Astronomical Observatory of Japan, 650 North Afohoku Place, Hilo, HI 96720, USA
[14]Department of Earth and Space Science, Graduate School of Science, Osaka University, Toyonaka, Osaka 560-0043, Japan
[15]Okayama Astrophysical Observatory, National Astronomical Observatory of Japan, Asakuchi, Okayama 719-0232, Japan
[16]Department of Particle and Astrophysical Science, Nagoya University, Chikusa-ku, Nagoya 464-8602, Japan
[17]Graduate School of Science and Engineering, Kagoshima University, Kogoshima 890-0065, Japan

© 2014. Astronomical Society of Japan.

[18]Department of Physics, Faculty of Science, Kyoto Sangyo University, 603-8555 Kyoto, Japan
[19]Mt. John University Observatory, Lake Tekapo 8770, New Zealand
[20]Research Center for the Early Universe, Graduate School of Science, The University of Tokyo, Bunkyo-ku, Tokyo 113-0033, Japan
[21]The Reseach Institute of Time Studies, Yamaguchi University, Yamaguchi 753-8511, Japan

*E-mail: yoshidam@hiroshima-u.ac.jp

Received ; Accepted

Abstract

We report the results of optical–infrared follow-up observations of the gravitational wave (GW) event GW151226 detected by the Advanced LIGO in the framework of J-GEM (Japanese collaboration for Gravitational wave ElectroMagnetic follow-up). We performed wide-field optical imaging surveys with Kiso Wide Field Camera (KWFC), Hyper Suprime-Cam (HSC), and MOA-cam3. The KWFC survey started at 2.26 days after the GW event and covered 778 deg^2 centered at the high Galactic region of the skymap of GW151226. We started the HSC follow-up observations from $\sim$12 days after the event and covered an area of 63.5 deg^2 of the highest probability region of the northern sky with the limiting magnitudes of 24.6 and 23.8 for i band and z band, respectively. MOA-cam3 covered 145 deg^2 of the skymap with MOA-red filter $\sim$2.5 months after the GW alert. Total area covered by the wide-field surveys was 986.5 deg^2. The integrated detection probability of all the observed area was $\sim$29%. We also performed galaxy–targeted observations with six optical and near-infrared telescopes from 1.61 days after the event. Total of 238 nearby ($\leq$100 Mpc) galaxies were observed with the typical I band limiting magnitude of $\sim$19.5. We detected 13 supernova candidates with the KWFC survey, and 60 extragalactic transients with the HSC survey. Two third of the HSC transients were likely supernovae and the remaining one third were possible active galactic nuclei. With our observational campaign, we found no transients that are likely to be associated with GW151226.

Key words: gravitational waves — black hole physics — surveys — methods:observational — binaries:close

1 Introduction

Gravitational wave (GW) is a quadrupole wave of space-time distortion propagating with the light speed. Strong GW is emitted by violent gravitational disturbance induced by a coalescence between compact massive objects such as neutron stars (NSs) or black holes (BHs). In order to observe GW directly, new generation GW detectors; Advanced LIGO (aLIGO, Abbott et al. 2016b), Advanced Virgo (aVirgo; Acernese et al. 2015), and KAGRA (Somiya 2012) are being constructed. If the planned sensitivities are achieved, these GW detectors can detect GW signals from an NS–NS merger at a distance of 200 Mpc (Abadie et al. 2010). The GW detection rate is anticipated to be in a range of 0.4–400 events yr^{-1} for NS–NS merger (Abadie et al. 2010). Uncertainty of the above number primarily comes from the limit of our knowledge on real number of NS binary fraction in a galaxy.

If a compact object merger contains one NS, wide wavelength range of electromagnetic (EM) emission associated with GW is expected (Li & Paczynski 1998; Rosswog 2005; Nakar & Piran 2011; Roberts et al. 2011; Metzger et al. 2010; Metzger & Berger 2012; Barnes & Kasen 2013; Hotokezaka et al. 2013; Tanaka & Hotokezaka ; Berger 2014; Tanaka et al. 2014). The EM emission would tell us important pieces of information about the nature of the GW event; its astrophysical origin, detailed localization, accurate distance, and local environment of the event. Most promising optical–near-infrared emission from GW sources is radioactively-powered emission, so called “kilonova” or “macronova” associated with NS–NS or BH–NS mergers (Metzger & Berger 2012; Barnes & Kasen 2013; Tanaka et al. 2014). A strong tidal force induced by merging process blows out the outer layer of NS, and a wide solid angle outflow from the merger emits a wide range of EM emission due to radioactive decay of the ejecta, that is “kilonova”. Neutron rich ejecta of a kilonova produce huge amount of r-process elements, thus the kilonova emission gives important clues to the long standing mystery about the sites of cosmic r-process nucleosynthesis. Moreover, the luminosity and light curve of a kilonova would allow us to constraint the

equation of state of NS. To search for EM emission associated with GW events, we organized an EM follow-up observation network J-GEM (Japanese collaboration of Gravitational wave Electro-Magnetic follow-up; Morokuma et al. 2016) by utilizing optical-infrared-radio telescopes of Japan.

The first direct detection of GW was achieved by aLIGO on Sep. 14 2015 (Abbott et al. 2016a). aLIGO performed the first science run (O1) from Sep. 2015 to Jan. 2016. Just before the regular operation of O1, aLIGO detected the GW at Sep. 14 2015 09:50:45 UT (Abbott et al. 2016a). The GW from this event, which was named as GW150914, was emitted by a 36 $M_\odot$–29 $M_\odot$ binary BH coalescence. While many electromagnetic (EM) follow-up observations were performed for GW150914 (Abbott et al. 2016d; Abbott et al. 2016e; Ackermann et al. 2016; Evans et al. 2016a; Kasliwal et al. 2016; Lipunov et al. 2016; Morokuma et al. 2016; Serino et al. 2016; Smartt et al. 2016a; Soares-Santos et al. 2016; Troja et al. 2016), no clear EM counterpart was identified with those observations except for a possible detection of γ-ray emission by $Fermi$ Gamma-ray Burst Monitor (GBM) (Connaughton et al. 2016). However, the $Fermi$ GBM detection was not confirmed by INTEGRAL observations (Savchenko et al. 2016).

aLIGO detected another GW signal during O1. This event was detected at 03:38:53 UT on Dec. 26 2015 and was named as GW151226. The false alarm probability of the event was estimated as $<10^{-7}$ ($>5\sigma$) and 3.5×10^{-6} (4.5σ) (Abbott et al. 2016c). The GW was also attributed to a BH–BH binary merger whose masses are $14.2^{+8.3}_{-3.7}$ $M_\odot$ and $7.5^{+2.3}_{-2.3}$ $M_\odot$. The final BH mass was $20.8^{+6.1}_{-1.7}$ $M_\odot$ and a gravitational energy of ~1 $M_\odot$ was emitted as GW. The distance to the event was 440^{+180}_{-190} Mpc (Abbott et al. 2016c).

Here, we report the EM counterpart search for GW151226 performed in the framework of J-GEM. We assume that cosmological parameters h_0, Ω_m, and Ω_λ are 0.705, 0.27, and 0.73, respectively (Komatsu et al. 2011) in this paper. All the photometric magnitudes presented in this paper are AB magnitudes.

2 Observations

We performed wide-field survey and galaxy targeted follow-up observations in and around the probability skymap of GW151226. The 90% credible area of the initial skymap created by BAYESTAR algorithm (Singer et al. 2014) was $\sim$1400 deg^2 (LSC and Virgo 2015). The final skymap was refined by LALInference algorithm (Veitch et al. 2015) and the 90% area is finally 850 deg^2 (Abbott et al. 2016c). We also made an integral field spectroscopy for an optical transient (OT) candidate reported by MASTER. The specifications of the instruments and telescopes we used for the follow-up observations are summarized in Morokuma et al. (2016).

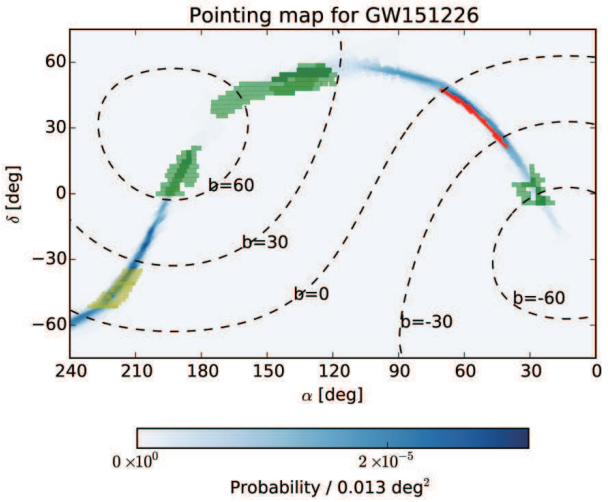

Fig. 1. The observed area of the wide-field surveys of the J-GEM follow-up observation of GW151226 overlaid on the probability skymap (dark blue scale). Green, red, and yellow colored regions represent the areas observed with KWFC, HSC, and MOA-cam3, respectively.

2.1 Wide Field Survey

We used three instruments for the wide-field survey; KWFC (Sako et al. 2012) on the 1.05 m Schmidt telescope at Kiso Observatory, HSC (Miyazaki et a. 2012) on the 8.2 m Subaru Telescope, and MOA-cam3 (Sako et al. 2008) on the 1.8 m MOA-II telescope at Mt. John Observatory in New Zealand.

The KWFC survey observations were done in r-band on Dec. 28 and 29 and Jan. 1–6 (UT). The total area observed with KWFC was 778 deg^2 far off the Galactic plane. To perform an image subtraction with the archival SDSS (Sloan Digital Sky Survey; Shadab et al. 2015) images, the high probability regions had to be avoided. Each field was observed typically twice or three times. The exposure time is 180 sec each and the seeing was 2.5–3.0 arcsec FWHM.

We carried out an imaging follow-up observations with HSC in the first half nights of Jan. 7, 13, and Feb. 6, 2016 (UT). We observed an area of 63.5 deg^2 centered at (α, δ) = (03:33:45, +34:57:14) spanning over the highest probability region in the initial skymap (BAYESTAR) with 50 HSC fiducial pointings. The fiducial pointings were aligned on a Healpix (Gorski, et al. 2005) grid with NSIDE=64 (a corresponding grid size is 0.84 deg^2). To remove artifacts efficiently, we visited each fiducial pointing twice with a 2 arcmin offset. We observed the field in i-band and z-band with an exposure time ranging from 45 sec to 60 sec for each pointing. On Feb. 6, first we surveyed all the fields by single exposure, then observed the whole area again. The seeing ranged from 0.5 arcsec to 1.5 arcsec FWHM.

We also performed survey observations with MOA-cam3 for a part of the skymap in the southern hemisphere from UT Mar. 8 to 11 2016. The total area covered by the MOA-cam3 observations was 145 deg^2. The "MOA-Red" filter (Sako et al.

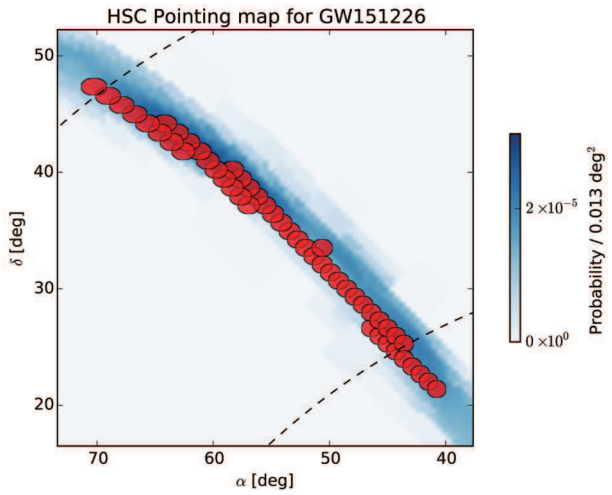

Fig. 2. The enlarged view of the survey area by HSC.

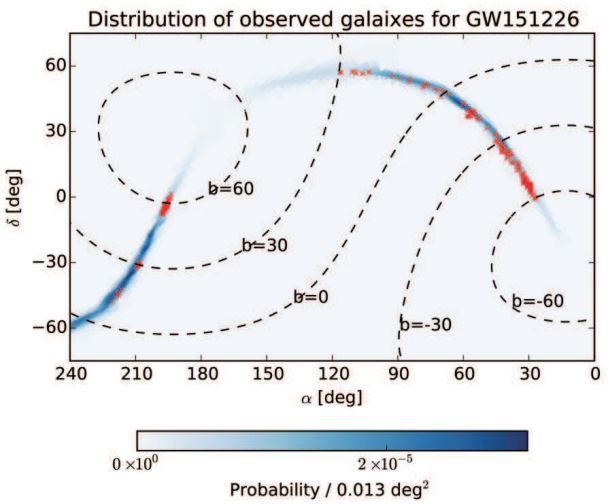

Fig. 3. The positions of the galaxies observed in the J-GEM follow-up observation of GW151226 (red points).

2008), which is a special filter dedicated to micro-lens survey with a wide range of transmission from 6200Å to 8100Å was used. The exposure time per field was 120 sec. The seeing was 1.9–4.5 arcsec FWHM.

Since the sky areas observed by the three instruments were not overlapped, the total area covered by the wide-field surveys was 986.5 deg^2. The integrated detection probabilities of the observed regions for the final skymap (LALInference) were 0.07, 0.09, and 0.13 for HSC, KWFC, and MOA-cam3, respectively. We thus covered a total of $\sim$29% of the probability skymap of GW151226.

The wide-field survey observations are summarized in Table 1. The survey areas and the probability skymap of GW151226 are shown in Figure 1. An enlarged map of the sky areas observed with HSC is shown in Figure 2.

2.2 Galaxy Targeted Follow-ups

We performed targeted follow-up imaging observations from UT Dec. 27 2015. We used seven instruments on six telescopes; HOWPol (Kawabata et al. 2008), HONIR (Akitaya et al. 2014) on 1.5 m Kanata telescope, MINT on 2 m Nayuta telescope, MITSuME (MITSuME-OAO) (Kotani et al. 2005) on 0.5 m telescope, OAO-WFC (Yanagisawa, et al. 2014) on 0.91 m telescope, MOA-cam3 on 1.8 m MOA-II telescope and SIRIUS (Nagayama et al. 2003) on 1.4 m IRSF, for these observations. We performed R band observations with HOWPol and MITSuME, I band observations with HOWPol, HONIR, and MINT, MOA-Red observations with MOA-cam3, J band observations with OAO-WFC, and J, H, and K bands observations with SIRIUS.

We selected 309 nearby galaxies from GWGC (Gravitational Wave Galaxy Catalog) (White, Daw & Dhillon 2011) in the skymap regions whose detection probabilities are more than 0.0008. We divided the target galaxies into 4 target groups. The groups 1 to 3 contain northern galaxies accessible from Japan. The number of galaxies of the group 1, 2, and 3 are 77, 76, and 77, respectively. The group 4 contains 79 southern galaxies. We allocated these groups to the above telescopes as target lists.

The summary of the targeted observations is shown in Table 2. The net number of the observed galaxies was 238. The spatial and distance distributions of the observed galaxies are shown in Figure 3 and Figure 4, respectively.

2.3 Spectroscopic Follow-up

We carried out a spectroscopic observation of MASTER OT J020906.21+013800.1 (Lipunov et al. 2015) with a fiber-fed integral field spectrograph KOOLS-IFU attached to the 188 cm telescope at Okayama Astrophysical Observatory on UT Dec. 28 2015. The field of view of KOOLS-IFU is 1.8 arcsec per fiber and 30 arcsec in total. The wavelength range and spectral resolving power were 5020–8830 Å and 600–850, respectively. The total exposure time was 3600 sec.

3 Data Reduction and Results

3.1 Wide Field Survey Data

3.1.1 KWFC survey

The data reduction of the KWFC data was made using the standard data reduction pipeline developed for Kiso Supernova Survey (KISS; Morokuma et al. 2014). The pipeline functions include bias subtraction, overscan subtraction, overscan trimming, flat-fielding, point spread function (PSF) size measurements, astrometry relative to the USNO-B1.0 catalog (Monet et al. 2003), zeropoint magnitude determination relative to the SDSS, image subtraction using the SDSS images, and detection

Table 1. The observing log of the wide field survey observations

Date (UT)	Instrument	mid-T[a] [days]	Area [deg^2]	Band	$m_{\rm lim}$[b] [AB mag]
2015-12-28	KWFC	2.43	176	r	19.2±1.3
2015-12-29	KWFC	3.48	512	r	19.5±0.3
2016-1-1	KWFC	6.59	48	r	17.1±1.2
2016-1-2	KWFC	7.67	124	r	20.3±0.2
2016-1-3	KWFC	8.70	56	r	20.1±0.3
2016-1-4	KWFC	9.49	84	r	19.9±0.3
2016-1-5	KWFC	10.36	40	r	19.8±0.6
2016-1-6	KWFC	11.60	124	r	20.0±0.2
2016-1-7	HSC	12.71	63.5	i, z	i: 24.3±0.2, z: 23.5±0.2
2016-1-13	HSC	18.17	63.5	i, z	i: 24.6±0.2, z: 23.8±0.2
2016-2-6	HSC	42.17	63.5	i, z	i: 24.4±0.2, z: 23.8±0.3
2016-3-8	MOA-cam3	73.31	55	MOA-red	18.2±0.1
2016-3-9	MOA-cam3	74.31	11	MOA-red	17.3±1.2
2016-3-10	MOA-cam3	75.35	117	MOA-red	18.2±0.3
2016-3-11	MOA-cam3	76.30	15	MOA-red	18.2±0.3

a. Middle time of the observation in unit of days after GW151226.

b. Median value of 5 σ limiting magnitude and its range (1σ) during one observation run.

Table 2. The average limiting magnitudes of the galaxy targeted observations

Date (UT)	Instruments	mid-T[a] [days]	$N_{\rm gal}$[b]	exp-T [sec]	$m_{\rm lim}$[c] [AB]
2015-12-27	HOWPol	1.67	18	90	R: 17.9±0.6, I: 18.3±0.4
2015-12-28	MITSuME	2.46	61	540	R: 18.5±0.4
	OAO-WFC	2.46	36	900	J: 18.3±0.3
	MINT	2.47	37	540	I: 20.1±0.5
	HONIR	2.49	51	120	I: 19.4±0.5
	SIRIUS	2.78	10	360–580	J: 19.3±0.4, H: 19.2±0.4, K: 18.1±0.4
2015-12-29	MITSuME	3.34	16	540	R: 18.5±0.4
	MOA-cam3	3.45	10	120	MOA-red: 17.3±0.7
	OAO-WFC	3.47	32	900	J: 16.4±0.4
	HONIR	3.49	20	120	I: 19.7±0.3
	MINT	3.53	38	540	I: 20.0±0.6
2015-12-31	MOA-cam3	5.39	29	120	MOA-red: 18.4±0.1
2016-01-04	MOA-cam3	9.40	24	120	MOA-red: 18.6±0.2
2016-01-05	MOA-cam3	10.30	19	120	MOA-red: 18.2±0.1

a. Middle time of the observation in unit of days after GW151226.

b. Number of observed galaxies.

c. Median value of 5 σ limiting magnitude and its range (1σ) during one observation run.

of transient candidates in the subtracted images. The 5σ limiting magnitudes of the KWFC observations ranged from 18.0 to 20.5 depending on the sky condition of the Kiso observatory.

The transient candidates detected in the subtracted images include not only astronomical objects but also non-astronomical artifacts, such as cosmic rays, residual of image subtraction due to imperfect image alignment or convolution (see e.g. Bailey et al. 2007; Bloom et al. 2012). Moreover, astronomical objects include minor planets or variable stars in addition to extragalactic transients. Therefore, we first removed the transient candidates around the objects which are registered as star in the SDSS catalog. This effectively removed both variable stars and artifacts around bright stars. Then, all the sources matched with the database of the Minor Planet Center were removed. Finally, the remaining objects were visually inspected to remove artifacts.

As a result, we found 13 extragalactic transient candidates associated with galaxies. The candidates found with the KWFC are summarized in Table 3. Nine out of 13 objects are detected more than twice in our survey. The other four objects (KISS15ah, KISS15ai, KISS16b, and KISS16c) were detected only once. Since KISS15ah and KISS16c are independently discovered by other groups (AT 2016bse and SN 2015bl, respectively), they must be genuine extragalactic transients. Although there is no independent discovery for KISS15ai and KISS16b, they are rather bright (16.6 and 19.6 mag, respectively), and unlikely to be minor planets which are not registered in the database of the Minor Planet Center.

In Table 3, we show estimated absolute magnitudes of 13

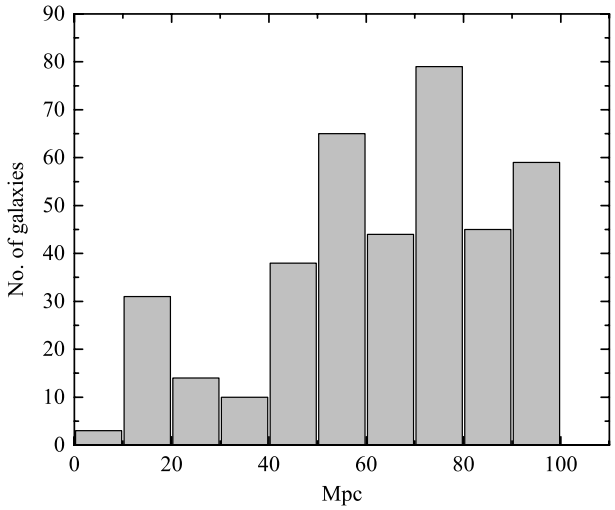

Fig. 4. The distance distribution of the observed galaxies. The distance limit (100 Mpc) of the galaxies is determined by GWGC.

transient candidates using spectroscopic and photometric redshifts. Except for KISS16f and KISS16b, the candidates were too bright for the expected kilonova emission (e.g. Tanaka et al. 2014), suggesting that they are supernovae (SNe). KISS16f and KISS16b were rather faint, but their host galaxies are located at z = 0.012 and 0.009964, respectively, and thus they were not associated with GW151226. They are likely to be SNe after the peak brightness.

3.1.2 HSC survey

The HSC data were reduced using HSC pipeline version 4.0.1, which had been developed based on the LSST pipeline (Ivezic et al. 2008; Axelrod et al. 2010). The HSC pipeline provides packages for bias subtraction, flat fielding, astrometry, mosaicing, warping, coadding, and image subtraction. The astrometry and photometry were made relative to the Pan-STARRS1 (PS1, Tonry et al. 2012; Schlafly et al. 2012; Magnier et al. 2013) with a 1.5 arcsec (9 pixel) aperture diameter. The limiting magnitudes were estimated by randomly sampling $> 10^5$ apertures.

The images taken on Feb. 6 were used as the reference images and were subtracted from the images taken on Jan. 7 and 13. Here, we separately adopted images at 2 epochs on Jan. 7, while images on Jan. 13 were coadded. Point sources in the difference images were detected and measured with the HSC pipeline. Since there were many false detections, we screened the detected sources by the following selection procedure. (1) In order to exclude false detections, we selected point sources detected in both of the z-band difference images on Jan. 7 at the same location with a signal-to-noise ratio of $> 5\sigma$, ellipticity of $>$0.8, and FWHM of 0.8–1.3 arcsec. In addition, a small residual of PSF subtraction from the sources ($< 3\sigma$) was imposed. (2) To select objects fading from Jan. 7 to Feb. 6, fluxes of sources in the two z-band difference images on Jan. 7 were required to be positive. (3) To exclude minor planets, first we estimated the maximum distance that an object could move during an interval between z- and i-band imaging observations. We found that it is $\sim$45 arcsec, assuming that the elongation in the z-band difference image was due to the movement of the object during the exposures. For the sources survived after the selections (1) and (2), we checked the i-band difference images. If a source was not detected but another transient source was found at a distance of 0.5–45 arcsec in i-band difference image, we omitted the source as a possible minor planet. We also check the position of sources with MPChecker.

After the above screening, 1256 candidates remained and were visually inspected. First, we removed clear artifacts from the candidate list by visual inspection. Then we identified and removed slowly moving objects which are thought to be distant minor planets not removed by the above criterion (3) by carefully checking the images. Finally, 60 objects remained as extragalactic transient candidates.

The multicolor light curves of the candidates were derived with forced aperture photometry of the difference images with 1.5 arcsec aperture diameter. We corrected the Galactic extinction using Schlegel et al. (1998).

We compared the color-magnitude time variations of variable component of the transient candidates between Jan. 7 and 13 with the color-magnitude evolutions of Type Ia, Ibc, and IIP SNe and kilonova emission and classified the candidates (Figure 5). For this comparison, we subtracted the brightnesses at 24 days and 30 days after the explosions from the model light curves of SNe and simulated the color-magnitude evolutions of the variable component of SNe. We adopted fiducial kilonova models of NS–NS merger with ejecta mass of 0.01 $M_\odot$ (model "APR4-1215" of Tanaka et al. 2014) and BH–NS merger with ejecta mass of 0.05 $M_\odot$ (model "H4Q3a75" of Tanaka et al. 2014).

By visual inspection and color-magnitude variation study, we found that two third of the HSC transients were probably SNe. One third of the HSC transients were located very close to the centers of the host galaxies and those time variabilities were not typical of SNe. We thus classified these sources as "active galactic nuclei (AGN)". No source whose color-magnitude variation is consistent with the kilonova models was identified by the above procedure. The extragalactic transient candidates found by the HSC survey are summarized in Table 4.

Morokuma et al. (2008) derived the number densities of various transient objects as a function of time interval of i' band observations from Subaru Suprime-Cam data in the Subaru/XMM-Newton Deep Field (Furusawa et al. 2008). According to Figure 12 of Morokuma et al. (2008), the number density of extragalactic transients (SNe + AGNs) brighter than the variable component i' magnitude $i'_{\rm vari}$ of 25 mag with 30 days interval observations is $\sim$30. The variable component

Table 3. The supernovae identified by the KWFC survey

ID	RA [deg]	DEC [deg]	T_{obs}(UT)[a]	m_r [AB]	m_{lim}[b] [AB]	host galaxy[c]	spec-z[d]	photo-z	M_r[e] [AB]
KISS15ag	141.812070	51.480666	2015-12-28 13:40:48	17.5	19.30	SDSS J092715.01+512853.2	0.053	-	−19.4
KISS15ah	140.142947	50.696334	2015-12-29 12:57:36	18.0	19.17	SDSS J092034.44+504148.7	-	0.050 or 0.063	−19.1
KISS15ai	19.249817	-4.942760	2015-12-29 09:50:24	16.6	20.00	SDSS J011659.36-045629.0	-	0.03	−19.1
KISS15aj	137.536390	50.061012	2015-12-29 12:14:24	17.4	19.37	UGC 04812	0.0343	-	−18.6
KISS16a	126.579910	53.770297	2016-01-02 18:28:48	18.7	20.40	SDSS J082619.18+534610.5	0.042	-	−17.8
KISS16b	140.725655	46.534659	2016-01-02 20:52:48	19.6	20.26	KUG0919+467	0.009964	-	−13.7
KISS16c	134.969736	53.265282	2016-01-02 19:55:12	19.3	20.46	SDSS J085952.59+531547.7	0.093	-	−18.9
KISS16d	136.815119	52.762845	2016-01-02 19:55:12	19.5	20.46	SDSS J090715.76+524544.6	NA	0.1	−18.9
KISS16e	131.618647	53.758743	2016-01-02 18:57:36	19.8	20.18	SDSS J084628.73+534531.2	-	0.10 or 0.08	−18.4
KISS16f	140.055455	54.108287	2016-01-03 20:38:24	18.5	20.16	SDSS J092012.28+540628.1	0.012		−15.2
KISS16g[f]	186.709112	16.263777	2016-01-03 20:09:36	19.7	20.41	SDSS J122649.70+161546.7	-	0.55 or 0.26	−22.1
KISS16h	126.292102	56.706847	2016-01-06 19:12:00	19.0	20.52	SDSS J082510.12+564222.5	0.043	-	−17.5
KISS16i	185.281171	16.935903	2016-01-06 20:09:36	19.7	20.41	SDSS J122107.48+165607.1	-	0.1	−18.7

a. Observation time (UT) of the events.

b. 5 σ limiting magnitude.

c. Closest galaxy in SDSS.

d. All the spectral redshifts except for KISS15aj and KISS16b were taken from SDSS DR12 (Shadab et al. 2015). The redshifts for KISS15aj and KISS16b were obtained from Fisher et al. (1995) and Falco et al. (1999), respectively.

e. When two values are given for photo-z, an average redshift is assumed.

f. Identification of the host galaxy is uncertain. The host galaxy may be SDSS J122650.23+161618.2 (z =0.046) located at about 29 arcsec north, and then the absolute magnitude of the transient is −16.1 mag.

i band limiting magnitude and the number density of the extragalactic transients in our work are ∼24 mag (see Table 4) and ∼1 deg^{-2}, respectively. Scaling the number density of Morokuma et al. (2008) using Figure 13 of (Morokuma et al. 2008), we estimate that it would be 3–4 deg^{-2} for the limiting magnitude $i'_{vari} \sim 24$ mag. This is a few times higher than the value of our observation. Part of this discrepancy would come from our detection strategy. We detected the transients based on z-band observation, thus we could systematically undercount blue transients. In addition, since the Galactic latitude b of the HSC observation field is less than ∼30 deg. (see Figure 1), large fraction of the field suffered from Galactic extinction (typical color excess $E(B-V)$ is ∼0.3–0.7; see Table 4). Considering these factors, we judge that our observation is roughly consistent with Morokuma et al. (2008).

3.1.3 MOA-II survey

The data of MOA-II were reduced in standard manner of CCD data reduction using IRAF. Astrometry of the data was done using Astrometry.net (Lang 2009). Then point source candidates were extracted with SExtractor (Bertin & Arnouts 1996). After excluding known stars using the USNO-B1.0 catalog, we omitted the candidates whose brightness profiles were not consistent with PSF by profile fitting using IRAF task ALLSTAR. We visually inspected the remaining 2953 candidates and selected 39 sources as transient object candidates. Then we checked 2MASS (Skrutskie et al. 2006) and WISE (Wright et al. 2010) images and found that 33 among the 39 candidates were 2MASS sources and one was a WISE source. Using Minor

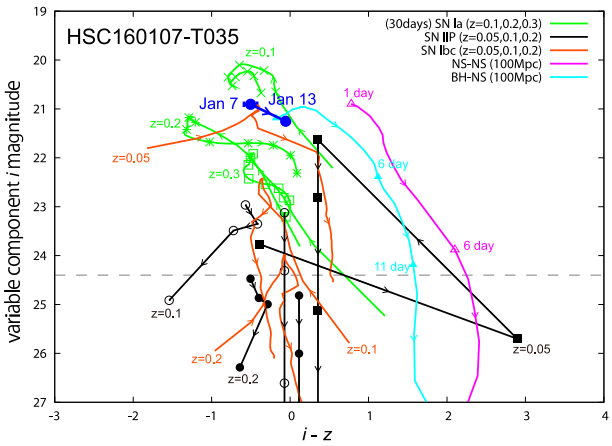

Fig. 5. Color-magnitude variation of variable component of a transient candidate of the HSC follow-up survey of GW151226. Filled blue circles are the data of HSC160107-T035 taken from Jan. 7 and 13 image after subtracting Feb. 6 image (Galactic extinction was corrected). Pink and light blue lines represent kilonova models of NS–NS merger and BH–NS merger of Tanaka et al. (2014) (see text). Green, black, and orange lines are the color-magnitude evolutions of variable components of SNe Type Ia, Type IIP, and Type Ibc, respectively. To derive the variable components of SNe, we subtracted the data 30 days after the explosions from the model light curves of SNe.

Planet Checker (MPChecker)[1], we found 3 candidates were asteroids. One of the candidates was a known supernova PSN J14102342-4318437.

After all selections, one candidate with $\sim$18.0 mag located at (α, δ) = (14:44:41.06, $-$44:4:38.4) remained. This source did not seem to be associated with bright galaxies. We observed this source twice with the interval of 180 sec on Mar. 10 2016 and did not detect significant motion of it between the two exposures. It completely disappeared at the third observation performed at the end of Aug. 2016. Though we cannot exclude the possibility that this source is an extragalactic transient, we think that the most plausible explanation is a minor planet not cataloged in MPChecker.

In the above processing, faint objects embedded in galaxies could be systematically lost. To detect such sources, we selected 2143 galaxies between 250 and 620 Mpc in the observed fields using GLADE (Galaxy List for the Advanced Detector Era)[2]. We found 549 point sources within 5 arcsec around these galaxies. Compared to DSS images, we found all the sources were known objects.

3.2 Galaxy Targeted Follow-up Data

The data reduction of the instruments used for the galaxy targeted observations — HOWPol, HONIR, MINT, MITSuME, MOA-II, OAO-WFC, and SIRIUS — was made in a standard manner; overscan correction, bias and dark subtraction, and flat-fielding. Then multiple exposure frames were coadded. The photometric calibrations of the optical data were made by comparing the fluxes of the field stars with those listed in the SDSS or GSC2.3 (Guide Star Catalog version 2.3). For the near-infrared bands data calibration, we used the 2MASS point source catalog (PSC) (Skrutskie et al. 2006). The observed galaxies and the limiting magnitudes of our observations are listed in Figure 1 of on-line supplementary data.

We searched for transient point sources in the observed frames taken with the above instruments by comparing them with DSS red frames for R and I bands, and with 2MASS PSC for near-infrared bands. We found transient candidates in I band frames of the galaxies PGC1202981 and UGC 1410 taken with HONIR on Dec. 28 2015. However, the former one was a Galactic variable star and the latter was a known minor planet. We also found a possible transient candidate close to the nucleus of PGC1021744 in a J band image taken with OAO-WFC on Dec. 28 2015. Since the source was slightly fainter than the 5σ limiting magnitude of the image ($\sim$17.2 mag), the detection was quite marginal. We made a follow-up observation for this object with OAO-WFC in the next night. The limiting magnitude of the observation reached 19.2 mag in J band with an exposure time of 2700 sec, but no point source was found at the same position. We thus could not confirm whether the source was a real astronomical transient.

As a conclusion, no extragalactic transient object was found with our galaxy targeted follow-up of GW151226.

3.3 Spectroscopic Follow-up Data

The target of the spectroscopy, MASTER OT J020906.21+013800.1, was reported at the unfiltered magnitude of 18.3 in the skymap area of GW151226 on UT Dec. 27 2015 and reported to be brightening (Lipunov et al. 2015). Our integral field spectroscopy found no significant signal from the OT candidate. Given that the radial intensity profile of the object is the Gaussian with FWHM of 3 arcsec, $\sim$40% of the object flux falls in 3 fibers. The 5σ limiting magnitude was 17.4 at 7400 Å. It is noted that the observations with the 3.6 m TNG starting on UT Dec. 28.8247 2015 also did not find any evidence for the OT with the upper limit of $r = 21.0$ mag (D'Avanzo et al. 2015). They detected the emission from a faint galaxy at the redshift of $\sim$0.034 at the position of the OT (D'Avanzo et al. 2015).

4 Discussion and Conclusion

No optical and near-infrared counterpart of the gravitational wave event GW151226 was identified by the follow-up observations under the J-GEM collaboration. Other teams' trials to find EM counterparts associated with this event also failed (Adriani et al. 2016; Cowperthwaite et al. 2016; Evans et al. 2016b; Racusin et al. 2016; Smartt et al. 2016b). We found 13 SNe candidates in the KWFC survey data, and 60 extragalactic transients in the HSC survey data. About two third of the HSC transients were probably SNe, and the remaining one third were classified as possible AGNs. There was no source which showed the color-magnitude variation consistent with current kilonova models in our dataset. We thus conclude that this work did not find clear candidates of EM counterpart of the gravitational wave source.

Both of the two GW events, GW150914 and GW151226, detected by aLIGO were BH–BH mergers. Inspired by the possible detection of a γ-ray emission associated with GW150914 by $Fermi$ satellite (Connaughton et al. 2016), several physical mechanisms for EM emission from a BH–BH merger event have been proposed (Morsony et al. 2016; Perna, Lazzti & Giacomazzo 2016; Yamazaki, Asano & Ohira 2016). However, all of those theoretical works have difficulties in producing strong EM emission by a BH–BH merger. In addition, questions have been raised for the reality of the γ-ray detection by $Fermi$ both from theoretical side (Lyutikov 2016; Zhang et al. 2016) and observational and data analysis side (Greiner et al.

[1] http://www.minorplanetcenter.net/cgi-bin/checkmp.cgi
[2] http://aquarius.elte.hu/glade

2016; Savchenko et al. 2016; Xiong 2016). Thus there is still no observational evidence with concrete theoretical background for EM emission from BH–BH merger. In other words, the key ingredient for detection of EM counterpart associated with GW is whether it contains a neutron star. Hence the information of the chirp mass of GW event is crucial for EM follow-up observations. When the chirp mass and distance estimation of a GW event is distributed, EM follow-up teams will be able to make effective observation plans with their available facilities (Singer et al. 2016).

For considering future observation strategies, we summarized the observation epochs and the limiting magnitudes of the J-GEM follow-up of GW151226 in Figure 6. The limiting magnitudes of R, r, I, i, and MOA-red bands taken with HOWPol, HONIR, MINT, MITSuME, MOA-cam3, KWFC, and HSC are plotted with theoretical i band light curves of kilonovae (Tanaka et al. 2014; Tanaka 2016). Our early observations with the small- and mid-sized- telescopes reached the depth of $\sim$20 mag in optical red bands. The KWFC data around 6–8 days after the GW event were as deep as $\sim$20.5 mag. The deepest data taken with HSC reached down to $\sim$24 mag in i band at 12 days after GW151226. According to the theoretical light curves in Figure 6, the depth of our early galaxy targeted observations reached the detection threshold of kilonova emission from a BH–NS merger within a distance of $\sim$50–100 Mpc. The late KWFC observations at around 7 days after the GW could follow the candidate. The deep HSC observations could follow the light curve of the candidate at most one month after the event.

However, if the event were NS–NS merger, the story would be completely changed. The kilonova emission for NS–NS merger is too faint to detect with our observations. Even if the event distance is 50 Mpc, the maximum magnitude of the optical emission would be much fainter than $\sim$19 mag at 1 day after the event. Only HSC could detect the optical emission from a kilonova at a distance of 50–100 Mpc if the follow-up observation with HSC was performed within $\sim$5 days after the event.

HSC has a capability to survey over $\sim$60 deg^2 with two colors, i and z bands, with the limiting magnitude of $\sim$24 mag within a half night. Figure 6 shows that quick ($<$3 days) follow-up observations with HSC can detect the optical emission of kilonova induced by an NS–NS merger at a distance of $\sim$200 Mpc. For BH–NS mergers, relatively slow start of the observation is acceptable. The kilonova EM emission from BH–NS merger at a distance of 400 Mpc would be detectable by HSC even after 10 days from the GW event. When aVirgo goes in regular operation and a joint observation of aLIGO and aVirgo starts, the 90% credible area of GW detection would become smaller than $\sim$50 deg^2 depending on the signal-to-noise ratio of the event (Singer et al. 2014). This size of area matches very well to the area covered by half night observation of HSC, and thus detection of EM emission from kilonova is greatly anticipated.

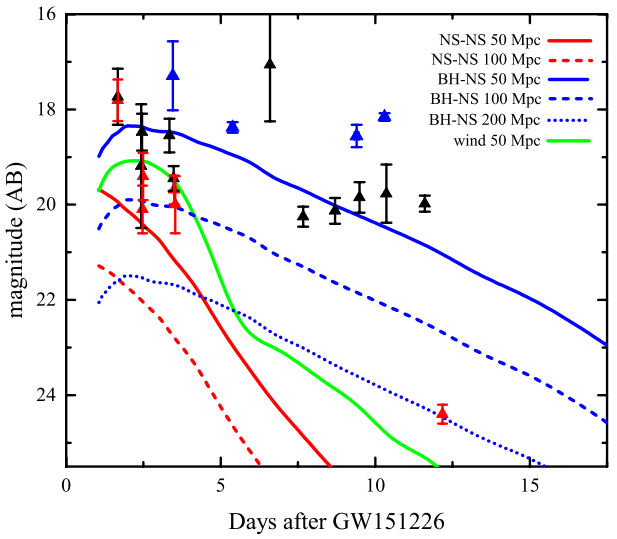

Fig. 6. The limiting magnitudes of the J-GEM observations of GW151226 and kilonova light curves. Filled triangles represent median 5σ limiting magnitudes and the y-axis error bars show the range of the variation of the limiting magnitudes in the observed data sets. Black, red, and blue colors represent R (r for KWFC) band, I (i for HSC) band, and MOA-red band, respectively. The theoretical i band light curves of NS–NS merger (APR4-1215 of Tanaka et al. 2014) and BH–NS merger (H4Q3a75 of Tanaka et al. 2014) are shown as red and blue lines, respectively. The green line shows the i band light curve of a model of the emission from shocked wind from NS–NS merger with ejecta mass of 0.03 $M_\odot$ (Tanaka 2016). Solid, dashed and dotted lines correspond to the event distance of 50 Mpc, 100 Mpc and 200 Mpc, respectively.

Acknowledgments

This work makes use of software developed for the Large Synoptic Survey Telescope. We thank the LSST Project for making their code available as free software at http://dm.lsstcorp.org. The Pan-STARRS1 Surveys (PS1) have been made possible through contributions of the Institute for Astronomy, the University of Hawaii, the Pan-STARRS Project Office, the Max-Planck Society and its participating institutes, the Max Planck Institute for Astronomy, Heidelberg and the Max Planck Institute for Extraterrestrial Physics, Garching, The Johns Hopkins University, Durham University, the University of Edinburgh, Queen's University Belfast, the Harvard-Smithsonian Center for Astrophysics, the Las Cumbres Observatory Global Telescope Network Incorporated, the National Central University of Taiwan, the Space Telescope Science Institute, the National Aeronautics and Space Administration under Grant No. NNX08AR22G issued through the Planetary Science Division of the NASA Science Mission Directorate, the National Science Foundation under Grant No. AST-1238877, the University of Maryland, and Eotvos Lorand University (ELTE). This research has made use of the NASA/IPAC Extragalactic Database (NED) which is operated by the Jet Propulsion Laboratory, California Institute of Technology, under contract with the National Aeronautics and Space Administration. This work was supported by MEXT Grant-in-Aid for Scientific Research on Innovative Areas "New Developments in Astrophysics Through Multi-Messenger Observations of Gravitational Wave Sources" (JP24103003), JSPS KAKENHI Grant Numbers JP26800103 and JP15H02069, and the

research grant program of Toyota foundation (D11-R-0830).

References

Abadie, J., et al. 2010, Classical and Quantum Gravity, 27, 173001
Abbott, B. P., et al. 2016a, Phys. Rev. Lett., 116, 061102
Abbott, B. P., et al. 2016b, Phys. Rev. Lett., 116, 131103
Abbott, B. P., et al. 2016c, Phys. Rev. Lett., 116, 241103
Abbott, B. P., et al. 2016d, ApJ, 826, L13
Abbott, B. P., et al. 2016e, ApJS, 225, 8
Acernese, E., et al. 2015, Classical and Quantum Gravity, 32, 024001
Ackermann, M., et al. 2016, ApJ, 823, L2
Adriani, O., et al. 2016, arXiv:1607.00233
Akitaya, H., et al. 2014, Proc. SPIE, Vol. 9147, 91474O
Axelrod, T., et al. 2010, SPIE, 7740, 774015
Bailey, S., et al. 2007, ApJ, 665, 1246
Barnes, J. & Kasen, D. 2013, ApJ, 775, 18
Bauswein, A., Goriely, S. & Janka, H.-T. 2013, ApJ, 773, 78
Berger, E. 2014, ARA&A, 52, 43
Bertin, E. & Arnouts, S. 1996, A&AS, 117, 393
Bloom, J. S., et al. 2012, PASP, 124, 1175
Connaughton, V., et al. 2016, ApJ, 826, L6
Cowperthwaite, P. S., et al. 2016, ApJ, 826, 29L
D'Avanzo et al. 2015, GCN Circular, 18775
Evans, P. A., et al. 2016, MNRAS, 460, 40
Evans, P. A., et al. 2016, arXiv:1606.05001
Falco, E. E., et al. 1999, PASP, 111, 438
Fisher, K. B., et al. 1995, ApJS, 100, 69
Furusawa, H., et al. 2008, ApJS, 176, 1
Gorski, K. M., et al. 2005, ApJ, 622, 759
Greiner, J., Burgess, J. M., Savchenko, V. & Yu, H.-F. 2016, arXiv:1606.00314
Grossman, D., Koroblin, O., Rosswog, S. & Piran, T. 2014, MNRAS, 439, 717
Hotokezaka, K., Kiuchi, K., Kyutoku, K., Muranushi, T., Sekiguchi, Y., Shibata, M. & Taniguchi, K. 2013, Phys. Rev. D, 87, 024001
Ivezic, Z., et al. 2008, http://www.lsst.org/files/docs/LSSToverview.pdf
Kasliwal, M. M., et al. 2016, ApJ, 824, 24
Kawabata, K. S., et al. 2008, Proc. SPIE, Vol. 7014, 70144L
Komatsu, E., et al. 2011, ApJS, 192, 18
Kotani, T., et al. 2005, Nuovo Cimento C Geophysics Space Physics C, 28, 755
Lang, D. 2009, Ph.D. Thesis, University of Toronto
Li, L.-X. & Paczynski, B. 1998, ApJ, 507, L59
LIGO Scientific Collaboration and Virgo Collaboration 2015, GCN Circular, 18728, 1
Lipunov, V. et al. 2015, GCN Circular, 18729, 1
Lipunov, V. M., et al. 2016, arXiv:1605.01607
Lyutikov, M. 2016, arXiv:1602.07352
Magnier, E. A., et al. 2013, ApJS, 205, 20
Metzger, B. D., et al. 2010, MNRAS, 406, 2650
Metzger, B. D. & Berger, E. 2012, ApJ, 746, 48
Miyazaki, S., et al. 2012, in Proc. SPIE, Vol. 8446, 84460Z
Monet, D. G., et al. 2003, AJ, 125, 984
Morokuma, T., et al. 2008, ApJ, 676, 163
Morokuma, T., et al. 2014, PASJ, 66, 114
Morokuma, T., et al. 2016, PASJ, 68, L9
Morsony, B. J., Workman, J., Jared, G. & Ryan, D. M. 2016, ApJ, 825, 24
Nakar, E. & Piran, T. 2011, Nature, 478, 82
Nagayama, T., et al. 2003, Proc. SPIE, Vol. 4841, 459
Perna, R., Lazzati, D., & Giacomazzo, B. 2016, arXiv:1602.05140
Racusin, J. L., et al. 2016, arXiv:1606.04901
Roberts, L. F., Kasen, D., Lee, W. H. & Ramirez-Ruiz, E. 2011, ApJ, 736, L21
Rosswog, S. 2005, ApJ, 634, 1202
Sako, S., et al. 2012, in Proc. SPIE, Vol, 8446, 844673
Sako, S., et al. 2008, Experimental Astronomy, 22, 51
Savchenko, V., et al. 2016, ApJ, 820, L36
Shadab, A., et al. 2015, ApJS, 219, 12
Schlafly, E. F., et al. 2012, ApJ, 756, 158
Schlegel, D. J., Finkbeiner, D. P. & Davis, M. 1998, ApJ, 500, 525
Serino, M., et al. 2016, GCN Circular, 19013, 1
Singer, L. P., et al. 2014, ApJ, 795, 105
Singer, L. P., et al. 2016, arXiv:1603.07333
Skrutckie, M. F., et al. 2006, AJ, 131, 1163
Smartt, S. J., et al. 2016a, arXiv:1602.04156
Smartt, S. J., et al. 2016b, arXiv:1606.04795
Somiya, K. 2012, Classical and Quantum Gravity, 29, 124007
Soares-Santos, M., et al. 2016, ApJ, 823, L33
Tanaka, M. & Hotokezaka, K. 2013, ApJ, 775, 113
Tanaka, M., Hotokezaka, K., Kyutoku, K., Wanajo, S., Kiuchi, K., Sekiguchi, Y. & Shibata, M. 2014, ApJ, 780, 31
Tanaka, M. 2016, Advances in Astronomy, 2016, id.634197
Tonry, J. L., et al. 2012, ApJ, 750, 99
Troja, E., Read, A. M., Tiengo, A. & Salvaterra, R. 2016, ApJ, 822, L8
Veitch, J., et al. 2015, Phys. Rev. D, 91, 042003
White, D. J., Daw, E. L., & Dhillon, V. S. 2011, Classical and Quantum Gravity, 28, 085016
Wright, E. L., et al. 2010, AJ, 140, 1868
Xiong, S. 2016, arXiv:1605.05447
Yamazaki, R., Asano, K. & Ohira, Y. 2016, PTEP, 2016, 051E01
Yanagisawa, K., et al. 2014, in Proc. SPIE, Vol. 9147, 91476D
Zhang, S.-N., Liu, Y., Yi, S., Dai, Z. & Huang, C. 2016, arXiv:1604.02537

Table 4. The extragalactic transients identified by the HSC survey

ID	RA [deg]	DEC [deg]	$E(B-V)$	$T_{\rm obs}(i)$[a]	m_i [AB]	$T_{\rm obs}(z)$[b]	m_z [AB]	type
HSC160107-T001	40.997379	22.369333	0.21	09:22:40	23.9	07:33:46	22.5	SN
HSC160107-T002	41.176235	22.611018	0.27	09:22:40	22.9	07:33:46	22.7	SN
HSC160107-T003	42.560811	23.350175	0.21	09:18:45	24.4	07:29:08	24.0	SN
HSC160107-T004	42.872344	22.315740	0.41	09:20:04	>24.2	07:30:41	22.2	SN
HSC160107-T005	43.455010	25.258338	0.12	09:12:10	>24.5	07:21:26	22.9	AGN
HSC160107-T006	43.507674	24.850162	0.12	09:11:31	>24.7	07:20:39	22.8	SN
HSC160107-T007	43.754581	23.637964	0.23	09:14:50	23.7	07:24:31	23.1	SN
HSC160107-T008	44.116261	24.054421	0.14	09:12:12	21.7	07:21:26	21.2	SN
HSC160107-T009	44.136838	25.945316	0.12	09:06:57	>24.0	07:15:12	21.7	SN
HSC160107-T010	44.364382	24.190641	0.13	09:11:32	24.0	07:20:39	22.8	AGN
HSC160107-T011	44.752975	26.107955	0.21	09:05:38	23.4	06:21:47	23.1	SN
HSC160107-T012	44.819914	24.395057	0.22	09:09:33	>23.9	07:18:20	22.2	AGN
HSC160107-T013	45.332537	25.263094	0.31	08:59:07	>24.7	05:21:51	23.0	AGN
HSC160107-T014	45.382080	24.835433	0.27	09:01:43	24.5	05:25:14	23.1	SN
HSC160107-T015	45.692939	26.530651	0.19	08:57:51	24.1	05:18:53	24.1	SN
HSC160107-T016	45.985724	27.425493	0.19	08:56:33	>25.0	05:18:28	22.3	AGN
HSC160107-T017	46.008330	25.975611	0.22	08:53:58	23.6	05:15:23	23.3	SN
HSC160107-T018	46.099802	27.108579	0.19	08:55:16	24.3	05:16:55	22.5	AGN
HSC160107-T019	46.346789	26.882343	0.21	08:55:16	22.5	05:16:55	22.4	SN
HSC160107-T020	46.462762	27.009164	0.21	08:56:20	21.6	05:18:12	21.2	SN
HSC160107-T021	46.830698	27.322635	0.21	08:53:58	>24.3	05:15:22	22.8	SN
HSC160107-T022	47.162617	28.111701	0.29	08:51:23	23.5	05:12:15	23.1	SN
HSC160107-T023	47.180281	28.363844	0.25	08:48:49	24.2	05:09:08	23.9	SN
HSC160107-T024	47.648348	28.246272	0.49	08:48:49	24.0	05:09:08	22.6	SN
HSC160107-T025	47.734609	28.924534	0.37	08:47:30	23.7	05:07:35	22.8	SN
HSC160107-T026	47.762266	29.189132	0.29	08:46:51	>24.3	05:06:49	22.7	SN
HSC160107-T027	48.584401	30.219543	0.37	08:41:28	>24.8	05:45:30	23.6	AGN
HSC160107-T028	48.878845	30.786932	0.37	08:37:52	21.7	07:11:24	21.5	SN
HSC160107-T029	50.365169	33.849423	0.24	08:40:38	21.0	04:59:49	20.8	SN
HSC160107-T030	50.453222	32.469045	0.41	08:28:22	>24.3	07:00:39	23.3	SN
HSC160107-T031	50.621347	32.624719	0.38	08:27:00	22.7	06:59:05	22.2	AGN
HSC160107-T032	50.830253	32.696495	0.40	08:25:38	>24.6	06:57:32	22.6	AGN
HSC160107-T033	50.892772	32.243608	0.38	08:27:00	23.1	06:59:05	23.1	SN
HSC160107-T034	51.672064	33.625310	0.27	08:18:53	23.0	06:50:19	22.6	AGN
HSC160107-T035	52.595560	35.179117	0.29	08:10:29	21.4	06:41:00	21.7	SN
HSC160107-T036	53.315983	35.731965	0.27	08:11:54	>24.7	06:42:33	23.6	SN
HSC160107-T037	53.909867	35.092927	0.34	08:11:54	23.9	06:42:33	23.5	SN
HSC160107-T038	54.092770	35.448804	0.30	08:11:54	>24.3	06:42:33	22.2	SN
HSC160107-T039	54.585872	37.015130	0.52	08:22:12	>24.1	06:53:56	22.4	SN
HSC160107-T040	54.912712	36.394118	0.44	08:22:12	>23.8	06:53:56	20.9	AGN
HSC160107-T041	55.370525	37.555876	0.44	08:52:46	>24.6	06:36:00	23.3	AGN
HSC160107-T042	55.632338	36.242112	0.49	08:22:12	>24.4	06:53:56	22.9	SN
HSC160107-T043	56.537885	38.800077	0.32	09:31:06	23.2	05:35:10	24.0	AGN
HSC160107-T044	56.639089	36.644814	0.40	09:33:41	23.2	05:38:16	22.8	SN
HSC160107-T045	56.898156	36.857295	0.36	09:33:41	22.1	05:38:16	22.7	AGN
HSC160107-T046	57.003385	36.936598	0.34	09:33:41	22.5	05:38:16	22.6	SN
HSC160107-T047	57.024877	36.695131	0.38	09:33:41	21.2	05:38:16	21.9	SN
HSC160107-T048	58.172853	37.840891	0.95	09:38:58	23.5	05:44:25	22.8	SN

Table 4. (Continued)

ID	RA	DEC	$E(B-V)$	$T_{\rm obs}(i)$	m_i	$T_{\rm obs}(z)$	m_z	type
	[deg]	[deg]			[AB]		[AB]	
HSC160107-T049	60.477172	39.860675	0.83	09:49:23	22.3	05:56:43	21.6	AGN
HSC160107-T050	62.176935	42.152778	0.58	09:58:26	23.4	06:07:32	23.6	SN
HSC160107-T051	63.477258	41.424544	0.73	09:59:44	23.2	06:09:05	$>$23.2	SN
HSC160107-T052	64.308645	42.773320	0.78	10:07:36	24.7	06:18:34	22.5	AGN
HSC160107-T053	64.875372	43.850244	0.79	10:10:14	25.1	06:21:41	23.0	AGN
HSC160107-T054	65.638499	43.614708	0.70	10:12:52	22.3	06:24:49	22.4	SN
HSC160107-T055	66.332247	44.279330	0.80	10:14:11	22.2	06:26:22	21.5	SN
HSC160107-T056	67.121767	45.254756	1.48	10:17:29	$>$24.3	06:29:26	20.7	AGN
HSC160107-T057	67.213427	45.250006	1.52	10:16:50	23.4	06:29:26	22.5	SN
HSC160107-T058	69.108532	46.036008	1.78	10:20:46	22.8	06:34:05	21.8	SN
HSC160107-T059	69.776861	46.009513	1.55	10:20:46	$>$24.5	06:34:05	22.2	SN
HSC160107-T060	69.983965	47.715348	1.40	10:23:25	22.8	06:37:13	21.2	AGN

a. Observation time (UT) in i band on Jan. 7 2016.

b. Observation time (UT) in z band on Jan. 7 2016.